Int. J. Heat Mass Transfer. Vol. 34, No. 6, pp. 1337–1346, 1991
Printed in Great Britain

0017-9310/91 $3.00+0.00

Finite difference simulation for heat conduction with phase change in an irregular food domain with volumetric change

SHIOWSHUH SHEEN and KAN-ICHI HAYAKAWA
Department of Food Science, Cook College, Rutgers University, P.O. Box 231, New Brunswick, NJ 08903, U.S.A.

(*Received* 30 *January* 1990 *and in final form* 5 *June* 1990)

Abstract—A mathematical model including the volumetric changes for food freezing or thawing is obtained by modifying the general heat conduction parabolic partial differential equation. The shape of food is assumed to be a body of rotation with an irregular cross-sectional contour. Coordinates are fixed to the initial food volume through a proper coordinate transformation. Due to the highly temperature-dependent food properties during phase change, the nodal temperatures are solved numerically by a general implicit finite difference method while a heat balance method is applied to boundary nodes with any kind of boundary conditions. A computerized numerical simulation method is developed and verified experimentally for a general heat conduction phase change (solidification/melting) problem.

INTRODUCTION

TRANSIENT heat conduction involving solidification and melting is important in many engineering applications, e.g. food freezing and thawing, ground freezing and metal casting. The exact solution of such a problem is difficult because of the moving interface between the solid and liquid phase when latent heat is absorbed or released. Although there are many methods available for solving these phase change or 'moving boundary' problems, they are usually only applicable to specific cases such as in an infinite or semi-infinite domain with simple initial and/or boundary condition [1–3]. When the material physical properties are functions of temperature, the analytical solutions for a finite irregular domain are almost impossible to obtain.

The numerical solutions (finite difference, finite element and boundary element methods) of heat conduction processes with phase change and with nonlinearity of material properties also present some difficulties. Lynch and O'Neil [4], and Yoo and Rubinsky [5] used a time-variable mesh finite element method, which explicitly traced the interface position, to solve the phase change problem. Although, the time-variable mesh approach often offers good accuracy, it is limited to simpler geometries. The finite difference solution of a heat conduction equation is usually confined to simple shape domains. Pham [6] proposed a fast, unconditionally stable finite difference scheme which avoids the jumping of the latent heat peak (temperature method with large time step) and eliminates the convergence problem and iterative procedures if enthalpy methods with explicit and implicit schemes were used, respectively. Although the finite element method is more flexible for an irregular domain than the finite difference method, Shamsundar and Rooz [7] point out that the computer time required by the finite element method is three times that by the finite difference method in the one-dimensional moving boundary case (freezing of a saturated liquid with constant wall heat flux). The advantages and disadvantages of both numerical methods for solving the moving boundary problems are also given and will not be repeated here. Recently, Saitoh and Kato [8] introduced a random point method (RPM) which utilizes randomly generated points around a pivotal point to formulate the governing equations. They claimed that no mesh generation is necessary and it can be applied to the three-dimensional moving boundary problem.

Many researchers have used numerical methods to solve heat conduction equations for freezing and thawing time estimation or process simulation in which the food properties are temperature dependent. Fleming [9] proposed a finite difference computer algorithm to simulate the food freezing processes which can be applied to irregular shapes. Unevenly discretized elements and stepwise constant thermal diffusivities over certain temperature intervals were applied. However, there was no report of detailed simulation results for irregular food. Purwadaria and Heldman [10] solved the heat conduction equation using the finite element method (two-dimensional simplex triangular elements) to simulate heat transfer in elliptical and trapezoidal shapes. They used a mass or area average enthalpy criterion to solve the equation. A generally applicable computer program was developed on ref. [11] to estimate heat transfer in an irregular shaped food undergoing freezing or thawing by using isoparametric finite elements. Succar and Hayakawa [12], Bonacina and Comini [13], Mannapperuma and Singh [14], Pham [15], and Cleland and Earl [16] also showed the freezing results

NOMENCLATURE

Bi Biot number [—]
B_m dimensionless modified mass transfer Biot number as defined [—]
C apparent specific heat [J kg^{-1} K^{-1}]
E empirical constant for apparent specific heat as defined [J kg^{-1} K^{-nc}]
e_x, e_1 x-directional cosine of an outward direction normal to boundary surface [—]
e_y, e_2 y-directional cosine of an outward direction normal boundary surface [—]
F view factor [—]
F_0 dimensionless process time as defined
H enthalpy of fusion [J kg^{-1}]
h convective heat transfer coefficient [W m^{-2} K^{-1}]
h_m convective mass transfer coefficient [(kg of water) s^{-1} m^{-2} Pa^{-1}]
k_x, k_y thermal conductivity of food in x- or y-direction [W m^{-1} K^{-1}]
k_{1x}, k_{1y} k_x, k_y values of food at unfrozen state [W m^{-1} K^{-1}]
k_{rx}, k_{ry} k_x, k_y values at reference temperature, 233.15 K
L latent heat of water vaporization or sublimation [J kg^{-1}]
L_v L/L_r [—]
l characteristic length of food [m]
m saturated pressure of water vapor at the food surface [Pa]
m_a partial pressure of water vapor in the surrounding medium [Pa]
NR dimensionless radiative heat transfer coefficient as defined [—]
P_c dimensionless apparent heat capacity [—]
p_d dimensionless density, ρ/ρ_r [—]
p_{kx} dimensionless thermal conductivity in x-direction [—]
p_{ky} dimensionless thermal conductivity in y-direction [—]
S food surface [m^2]
S_{ds} empirical constant as defined [kg m^{-3} K^{-1}]
S_{k1x}, S_{k1y} empirical constants for x- and y-directional thermal conductivity estimation, respectively, as defined [J s^{-1} m^{-2} K^{-1}]
S_{ksw} empirical constant as defined [J s^{-1} m^{-2} K^{-1}]
S_0 food surface at its initial temperature [m^2]
T temperature [K]
T_{ar} reference surrounding medium temperature, 233.15 K
T_{0r} reference initial temperature, 281.15 K
T_{sw} freezing point of pure water [K]
t time [s]
U dimensionless temperature [—]
U_s $T_{ar}/(T_{0r} - T_{ar})$ [—]
V food volume [m^3]
V_0 food volume at its initial temperature state [m^3]
x, y, z coordinates as functional of local temperature [m]
x_0, y_0 reference coordinates corresponding to the initial food temperature [m].

Greek symbols

α_r thermal diffusivity at T_{ar} [m^2 s^{-1}]
γ x-directional expansion factor [—]
δ ratio of x-directional thermal conductivity to y-directional one [—]
ε emissivity of material [—]
$\eta(x_0, y_0, z_0)$ directional linear expansion factors in three directions [—]
Θ angle between normal directional outward axis and x- or ξ-axis
$\Delta\theta$ radius of a small controlled volume [—]
ν ratio of z- to x-directional expansion factor in Cartesian system [—]
ξ, ζ dimensionless coordinates corresponding to x and y [—]
ρ density as functional of temperature [kg m^{-3}]
σ Stefan–Boltzmann constant [J s^{-1} m^{-2} K^{-4}]
Φ dimensionless parameter for m [—]
ω ratio of y- to x- (or z- to r-)directional expansion factor [—].

Subscripts

a ambient
c specific heat capacity
d density
e heat sink
l food property at unfrozen state
r reference temperature, 233.15 K (or −40°C)
s surface
sh initial freezing point of food
x, ξ x- or ξ-axis
y, ζ y- or ζ-axis
0 initial food temperature.

Superscripts

nc empirical constant for apparent specific heat as defined [—]
p index of y-axis rotation [—].

using finite difference techniques in simple shaped foods. Cleland *et al.* [17] reported that the computer time required for the simulation of a rectangular brick by the finite element method ($7\times7\times7$ node grid with 216 evenly sized, eight-node, linear isoparametric elements) was at least ten times greater than that for the finite difference method ($9\times9\times9$ evenly spaced node grid) according to their food freezing simulation.

Welty [18] recommended the application of a heat balance method together with a traditional finite difference technique for freezing and thawing process simulations. Rosenau [19] found that ten nodal points are sufficient for the simulation of one-dimensional freezing time estimation by considering the heat balance of each shell volume of an infinite cylinder. However, there is no one taking into account the volumetric change in the food freezing/thawing simulation research.

As observed by Cleland *et al.* [17], the use of a proper finite difference method reduced the computer time required to obtain a heat conduction solution considerably. Therefore, a finite difference method was used for the present study. The objectives of this investigation were: (i) to develop a computerized method, which can be applied to general heat conducting phase change problems, for freezing/thawing simulation in an irregular food domain with realistic assumptions of food properties including change of volume (two dimensions), (ii) to verify the developed procedures by freezing/thawing experiments.

MATERIALS AND METHODS

Mathematical model development

The governing partial differential equation generally applicable to heat conduction in the anisotropic food and its corresponding initial and boundary conditions are shown below [3].

Heat conduction equation.

$$x^p\rho C(\partial T/\partial t)=\frac{\partial}{\partial x}[x^p k_x(\partial T/\partial x)]+\frac{\partial}{\partial y}[x^p k_y(\partial T/\partial y)]$$
$$\text{for } t>0 \quad \text{and} \quad (x,y)\in V \qquad (1)$$

where $p=1.0$ for axisymmetric heat conduction and x becomes the radial direction axis; otherwise $p=0$. It should be noted that C in equation (1) is the apparent specific heat which includes the latent heat of freezing or thawing. The following boundary condition, equation (2), which is similar to the one considered in ref. [11] was applied.

Boundary condition.

$$k_x e_x\,\partial T/\partial x+k_y e_y\,\partial T/\partial y = -h(T_s-T_a)-\sigma F\varepsilon(T_s^4-T_e^4)-h_m L(m-m_a)$$
$$\text{for } t>0 \quad \text{and} \quad (x,y)\in S. \qquad (2)$$

Initial condition.

$$T=T_0 \quad \text{for } t=0 \quad \text{and} \quad (x,y)\in V \text{ and } S. \qquad (3)$$

No supercooling was assumed in the above equation since freezing of most foods proceed at a slow rate. All physical properties are assumed to be temperature dependent. The coordinates, fixed to current food volume, x and y, are time variable because of a volumetric change due to freezing and thawing. In order to estimate properly the apparent specific heat of a food material, the equation proposed by Comini and Del Giudice [20] by using an enthalpy gradient was applied and is shown below

$$C=\mathrm{d}H/\mathrm{d}T = [(\partial H/\partial x)(\partial T/\partial x)+(\partial H/\partial y)(\partial T/\partial y)]/[(\partial T/\partial x)^2+(\partial T/\partial y)^2]. \qquad (4)$$

Since there always exists a sharp peak in the apparent specific heat value at the initial freezing point of high moisture content materials due to phase change, integration of $\mathrm{d}H/\mathrm{d}T$ around the initial freezing point avoids missing the peak value. Equation (4) was also used in ref. [12] with good simulation results being reported. However, when the temperature gradient is very small (<0.001°C), C was obtained directly from the following empirical formula [12]:

$$C=C_1 \qquad \text{for } T\geqslant T_{sh}$$
$$C=C_r+E/(T_{sw}-T)^{nc} \qquad \text{for } T<T_{sh}. \qquad (5)$$

The empirical equations for thermal conductivity and density given in ref. [12] are also shown as

$$k_x=k_{1x}+S_{k1x}(T-T_{sh}) \qquad \text{for } T\geqslant T_{sh}$$
$$k_x=k_{rx}+S_{ksx}(T_{sh}-T)+(k_{1x}-k_{rx})(T_{sw}-T_{sh})/(T_{sw}-T) \qquad \text{for } T<T_{sh}$$
$$k_y=k_{1y}+S_{k1y}(T-T_{sh}) \qquad \text{for } T\geqslant T_{sh}$$
$$k_y=\delta k_x \qquad \text{for } T<T_{sh}$$

where

$$\delta=k_{1y}/k_{1x} \qquad (6)$$

$$\rho=\rho_1 \qquad \text{for } T\geqslant T_{sh}$$
$$\rho=\rho_r+S_{ds}(T_{sh}-T)+(\rho_1-\rho_r)(T_{sw}-T_{sh})/(T_{sw}-T) \qquad \text{for } T<T_{sh}. \qquad (7)$$

Equations (1)–(3) are difficult to solve since x and y are time dependent due to freezing or thawing change in the solution domain as mentioned previously. Therefore, they were expressed in terms of coordinates fixed to initial food volume, x_0 and y_0. The coordinate transformations are given below using Cartesian coordinates as an example

$$\mathrm{d}x=\eta_{x_0}\,\mathrm{d}x_0; \quad \mathrm{d}y=\eta_{y_0}\,\mathrm{d}y_0 \quad \text{and} \quad \mathrm{d}z=\eta_{z_0}\,\mathrm{d}z_0 \qquad (8)$$

where η_{x_0}, η_{y_0} and η_{z_0} are the x-, y- and z-directional, linear expansion factors which are dependent on local temperature.

Let

$$\eta_{y_0}/\eta_{x_0}=\omega; \quad \eta_{z_0}/\eta_{x_0}=\nu.$$

Then

$$(\rho_0/\rho) = \omega v(\eta_{x_0})^3$$

$$\therefore \eta_{x_0} = [\rho_0/(\omega v\rho)]^{1/3}$$

and

$$\eta_{y_0} = \omega\eta_{x_0}; \quad \eta_{z_0} = v\eta_{x_0}. \tag{9}$$

Therefore, from equations (8) and (9), we obtain

$$x = \int [\rho_0/(\rho\omega v)]^{1/3}\,\mathrm{d}x_0$$

$$y = \int v[\rho_0/(\rho\omega v)]^{1/3}\,\mathrm{d}y_0$$

$$z = \int v[\rho_0/(\rho\omega v)]^{1/3}\,\mathrm{d}z_0. \tag{10}$$

Thus, the modified governing equation (for cylindrical coordinates: x_0 replaced by r_0 and y_0 replaced by z_0) is given as

$$\left(\int \eta_{x_0}\,\mathrm{d}x_0\right)^p \rho C[\partial T/\partial t]$$

$$= (1/\eta_{x_0})\frac{\partial}{\partial x_0}\left[\left(\int \eta_{x_0}\,\mathrm{d}x_0\right)^p \frac{k_{x_0}}{\eta_{x_0}}\frac{\partial T}{\partial x_0}\right]$$

$$+ (1/\eta_{y_0})\frac{\partial}{\partial y_0}\left[\left(\int \eta_{x_0}\,\mathrm{d}x_0\right)^p \frac{k_{y_0}}{\eta_{y_0}}\frac{\partial T}{\partial y_0}\right]$$

$$\text{for } t > 0 \quad \text{and} \quad (x_0, y_0) \in V_0. \tag{11}$$

Boundary condition.

$$(1/\eta_{x_0})k_{x_0}e_{x_0}\partial T/\partial x_0 + (1/\eta_{y_0})k_{y_0}e_{y_0}\partial T/\partial y_0$$

$$= -h(T_s - T_a) \quad \text{(convective term)}$$

$$-\sigma F\varepsilon(T_s^4 - T_c^4) \quad \text{(radiative term)}$$

$$-h_m L(m - m_a) \quad \text{(moisture loss)}$$

$$\text{for } t > 0 \quad \text{and} \quad (x_0, y_0) \in S_0. \tag{12}$$

Initial condition.

$$T = T_0 \quad \text{for } t = 0 \quad \text{and} \quad (x_0, y_0) \in V_0 \text{ and } S_0. \tag{13}$$

In order to facilitate the further calculation, those equations were converted to the dimensionless form.

Let

$$U = (T - T_{ar})/(T_{0r} - T_{ar}); \quad \xi = x_0/l; \quad \zeta = y_0/l;$$

$$F_0 = (\alpha_r t)/l^2; \quad \alpha_r = k_{rx}/(\rho_r C_r); \quad P_{kx} = k_x/k_{rx};$$

$$P_{ky} = k_y/k_{ry}; \quad P_d = \rho/\rho_r; \quad P_c = C/C_r;$$

$$Bi = hl/k_{rx}; \quad NR = \sigma F\varepsilon l(T_{0r} - T_{ar})^3/k_{rx};$$

$$B_m = h_m L_r l m_r/[K_{rx}(T_{0r} - T_{ar})];$$

$$L_v = L/L_r; \quad \Phi = m/m_r;$$

and

$$\eta_{x_0} = \gamma \text{ (or } \eta_{r_0} = \gamma).$$

Therefore, the following equations were obtained:

governing equation

$$\gamma\left(\int \gamma\,\mathrm{d}\xi\right)^p P_d P_c(\partial U/\partial F_0) = \frac{\partial}{\partial\xi}\left[\left(\int \gamma\,\mathrm{d}\xi\right)^p \frac{P_{kx}}{\gamma}\frac{\partial U}{\partial\xi}\right]$$

$$+ \frac{K_{ry}}{\omega K_{rx}}\frac{\partial}{\partial\zeta}\left[\left(\int \gamma\,\mathrm{d}\xi\right)^p \frac{P_{ky}}{\omega\gamma}\frac{\partial U}{\partial\zeta}\right]; \tag{14}$$

boundary condition

$$\frac{P_{kx}e_1}{\gamma}(\partial U/\partial\xi) + \frac{K_{ry}P_{ky}}{K_{rx}\gamma\omega}e_2(\partial U/\partial\zeta)$$

$$= -Bi(U_s - U_a) - NR[(U_s + U_v)^4 - (U_c + U_v)^4]$$

$$- B_m L_v(\phi - \phi_a); \tag{15}$$

initial condition

$$U(\xi, \zeta, 0) = U_0(\xi, \zeta). \tag{16}$$

The moisture content in most frozen foods is fairly high and a small fraction of moisture is lost (or gained) during freezing or thawing (i.e. water activity of food remaining at unity). It was assumed that the thermodynamic properties of water in the food were identical to the saturated pure water. Therefore, the following equations were used for the present work [21].

Latent heat of vaporization or sublimation

$$L/1000 = \begin{cases} 2500.8 - 2.3668T & \text{when } T \geqslant T_{sb} \\ 2837.0 & \text{when } T < T_{sb} \end{cases} \tag{17}$$

Water vapor pressure:

when $T > T_{sb}$

$$\ln(m/1000) = -5674.5359/T$$

$$+ 6.3925247 - 0.9677843(10^{-2})T$$

$$+ 0.62215701(10^{-6})T^2 + 0.20747825(10^{-8})T^3$$

$$+ 0.9484024(10^{-12})T^4 + 4.1635019\ln(T) \tag{18}$$

when $T \leqslant T_{sb}$

$$\ln(m/1000) = -5800.2206/T$$

$$+ 1.3914993 - 0.04860239T + 0.41764768(10^{-4})T^2$$

$$- 0.14452093(10^{-7})T^3 + 6.5459673\ln(T). \tag{19}$$

It should be mentioned that T in equations (17)–(19) is in degree Celsius.

NUMERICAL METHODS

The solution domain was divided into non-uniformly spaced finite difference grids in which the regions of steep temperature gradients were divided into finer grids. An alternative directional implicit (ADI) [22] finite difference method was applied initially to solve equations (14)–(16). However, temperatures at the boundary nodes on a curvilinear sur-

face contour converged to grossly incorrect solutions (i.e. temperature below the surrounding medium temperature during cooling treatment), no matter how small the ratio of Δx, Δt and $k/c\rho$ values in a convergence criterion of 0.01, a relative temperature difference of two successive iterations was used. To eliminate this problem, a finite volume approximation procedure was applied to each boundary node and a finite difference approximation procedure [23] to each internal node.

There are two cases of boundary node arrangements which are sufficient to cover all different types of boundary contours (Fig. 1). The following equations were obtained through the consideration of energy balance in a finite volumetric element around a boundary node.

Energy balance analysis at the boundary node

Case 1 : (*referred to Fig.* 1).

Rate of energy input − Rate of energy output = Rate of energy accumulation

$$-k_x\Delta y[(x-0.5\Delta x)\Delta\theta](\partial T/\partial x) - k_y\Delta x(x\Delta\theta)(\partial T/\partial y) - \{h(T_s-T_a)+\sigma F\varepsilon(T_s^4-T_e^4) + h_m L(m-m_a)\}[(\Delta x^2+\Delta y^2)^{0.5}(x\Delta\theta)] = 0.5(\Delta x\,\Delta y)(x\Delta\theta)\rho C(\partial T/\partial t). \quad (20)$$

When Δx is small and original coordinates (x_0, y_0) are used as the reference coordinates, then equation (20) can be converted to dimensionless form equation (21).

Let

$$(\gamma\Delta\xi)/[(\gamma\Delta\xi)^2+(\omega\gamma\Delta\zeta)^2]^{0.5} = \cos\Theta = e_1$$

$$(\gamma\omega\Delta\zeta)/[(\gamma\Delta\xi)^2+(\omega\gamma\Delta\zeta)^2]^{0.5} = \sin\Theta = e_2$$

where Θ is the angle between the normal directional outward axis and the x- or ξ-axis

$$-[P_{kx}e_1/\gamma](\partial U/\partial\xi) - [(P_{ky}K_{ry}e_2)/(\gamma\omega K_{rx})](\partial U/\partial\zeta) - Bi(U_s-U_a) - NR[(U_s+U_v)^4-(U_e+U_v)^4] - B_m L_v(\phi-\phi_a) = 0.5|e_1|(\gamma\Delta\xi)P_d P_c(\partial U/\partial F_0) \quad (x\text{- or } \xi\text{-direction})$$

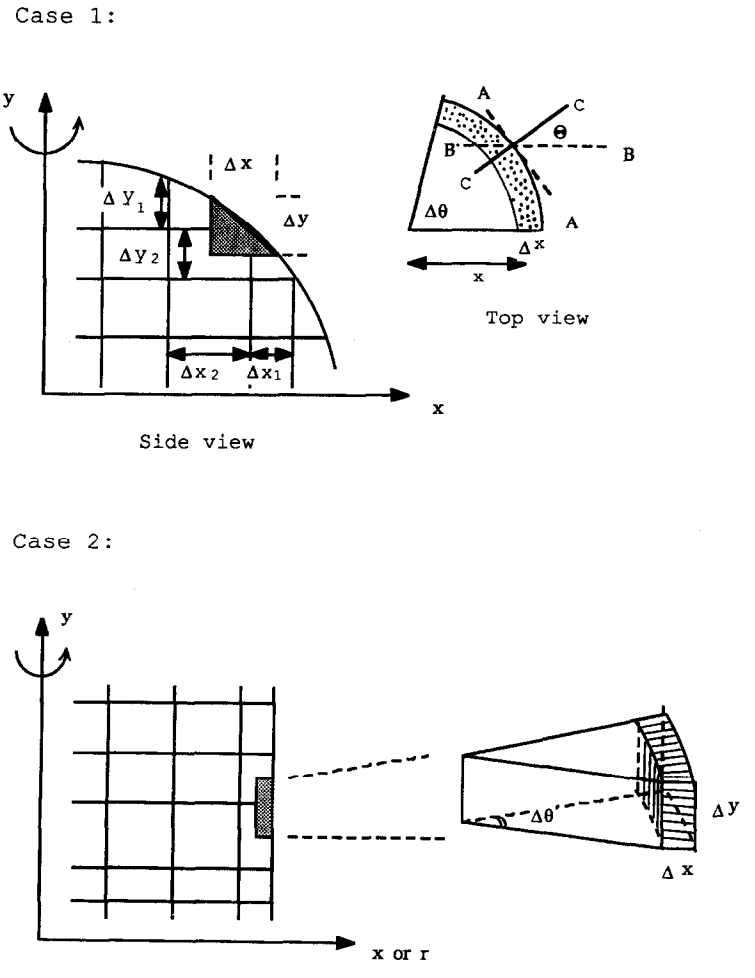

FIG. 1. The controlled volume at the boundary node.

or

$$-[P_{kx}e_1/\gamma](\partial U/\partial\xi)-[(P_{ky}K_{ry}e_2)/(\gamma\omega K_{rx})](\partial U/\partial\zeta)-Bi(U_s-U_a)-NR[(U_s+U_v)^4-(U_c+U_v)^4]-B_mL_v(\phi-\phi_a)=0.5|e_2|(\gamma\omega\Delta\xi)P_dP_c(\partial U/\partial F_0)\quad(y\text{- or }\zeta\text{-direction}).\tag{21}$$

Case 2: (*referred to Fig.* 1).

$$-K_x\Delta y[(x-0.5\Delta x)\Delta\theta](\partial T/\partial x)-[K_y\Delta x(x\Delta\theta)(\partial T/\partial y)|_y+K_y\Delta x(x\Delta\theta)(\partial T/\partial y)|_{y+\Delta y}]-\{h(T_s-T_a)+\sigma F\varepsilon(T_s^4-T_c^4)+h_mL(m-m_a)\}[\Delta y(x\Delta\theta)]=(\Delta x\Delta y)(x\Delta\theta)\rho C(\partial T/\partial t).\tag{22}$$

When Δx is small, equation (22) becomes (dimensionless)

$$-\frac{P_{kx}}{\gamma}\left(\frac{\partial U}{\partial\xi}\right)-\frac{\Delta\xi}{\omega}\left(\frac{K_{ry}}{K_{rx}}\right)\frac{\partial}{\partial\zeta}\left[\frac{P_{ky}}{\gamma\omega}\left(\frac{\partial U}{\partial\zeta}\right)\right]-Bi(U_s-U_a)-NR[(U_s+U_v)^4-(U_c+U_v)^4]-B_mL_v(\phi-\phi_a)=(\gamma\Delta\xi)P_dP_c(\partial U/\partial F_0)\quad(x\text{- or }\xi\text{-direction})$$

or

$$-(\omega\Delta\zeta)\frac{\partial}{\partial\xi}\left[\frac{P_{kx}}{\gamma}\left(\frac{\partial U}{\partial\xi}\right)\right]-\frac{P_{ky}K_{ry}}{\gamma\omega K_{rx}}\left(\frac{\partial U}{\partial\zeta}\right)-Bi(U_s-U_a)-NR[(U_s+U_v)^4-(U_c+U_v)^4]-B_mL_v(\phi-\phi_a)=(\gamma\omega\Delta\zeta)P_dP_c(\partial U/\partial F_0)\quad(y\text{- or }\zeta\text{-direction}).\tag{23}$$

Equations (21) and (23), not equation (15), were used together with the governing equation and initial condition for numerical solutions.

As stated previously, an ADI method was used to solve equations (14), (16) and (21) or (23). The difference equations, which can be found elsewhere [24], were not shown in which the thermal conductivity and coordinate change were the average values of two adjacent nodes.

Unfortunately, the unknown values of U in the boundary term for radiative heat transfer and moisture loss (equations (18) and (19)) are difficult to separate. Therefore, there are unknown temperature terms to be updated during the calculation. This problem can be solved with iteration without any difficulty. A similar principle was used in the ξ-directional integration.

The grid nodal points for each row and column should be properly classified, since a different type of boundary node might need different treatment. Figure 2 shows the two cases of arrangement for the ξ-directional integration:

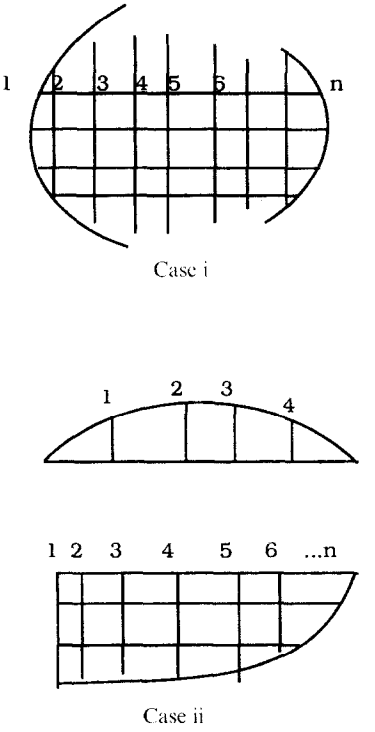

FIG. 2. Classification of nodal points for x- or ξ-directional integration. Case i, all internal nodes except two end points. Case ii, all boundary nodes: upper, curvilinear boundary; lower, straight line boundary.

(i) there is one boundary point at each end (the typical type);

(ii) all nodal points are boundary nodes where each point was treated as the 'internal node' except two end nodes, but the boundary condition was applied to each 'internal node'.

The same classification is applicable to the ζ-directional integration. The application of the stated methods resulted in simultaneous, first-order algebraic equations with a tridiagonal coefficient matrix the elements of which are functions of local temperature. The solution may be easily estimated through iterative computations [12, 25]. Updated nodal point temperatures were obtained through each iterative integration, the convergence criterion was a relative temperature difference of two successive iterative results at each time step. These integrations were in the forward finite difference form for first-order time derivative and the central finite difference form for the second-order space derivative. After all the ξ-directional integration was completed, the ζ-directional integration was performed to update nodal temperatures after another F_0 increment by ΔF_0. The procedures were repeated alternatively in the subsequent time steps until the final process temperature was reached.

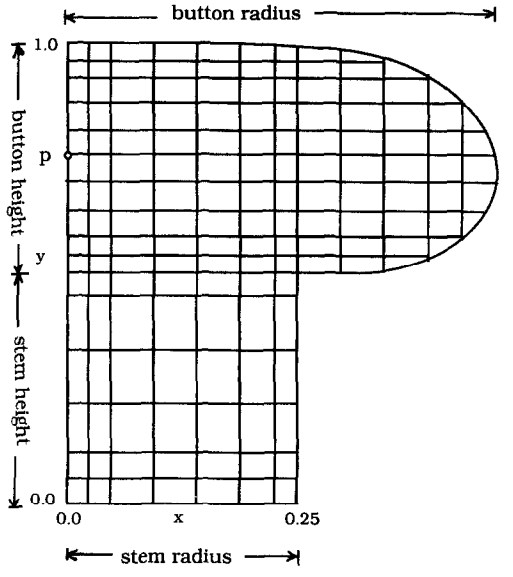

FIG. 3. Nodal point design for mushroom-shaped domain (one half). x-Coordinates are twice as large as their real size for better illustration. Point p is the location of the thermocouple.

EXPERIMENTAL VERIFICATION

The developed computer program was used to simulate heat conduction in a sample of mushroom or spheroidal shape. The nodal arrangements and sizes of each sample are shown in Figs. 3 and 4 for the mushroom shape and spheroid, respectively. In order to verify simulation results, a Karlsruhe [26] food simulator was used since its thermophysical properties are available and all the parameters for those formulae of temperature-dependent physical properties, equations (5)–(7), can be obtained from ref. [11]. The simulator was made from crystallized methyl-cellulose gel (77% moisture content). Molds for making mushroom-shaped and spheroidal samples were fabricated from the hydrate of Gypsum powders. A polyethylene (PE) film (0.0254 mm) was used to wrap each sample in order to minimize moisture loss at the surface.

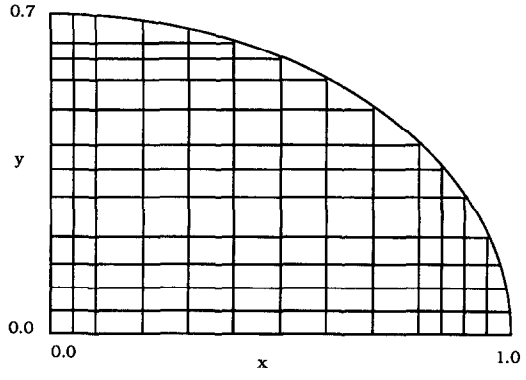

FIG. 4. Nodal point design for a spheroid domain (one quarter, y is the rotating axis).

A wind tunnel (0.31 m diameter and 2.025 m long) was designed for this experiment in which a centrifugal fan, located at one end provided the desired forced air flow. The fan rotor (0.31 m diameter) has a maximal capacity of supplying 55 $m^3 min^{-1}$ air flow. A sample, which had been placed in an incubator for 24 h to obtain a uniform initial temperature, was hung by thin thread in the middle of the wind tunnel 0.62 m from the outlet (the rotation axis of the sample was perpendicular to the air flow). A thermocouple (copper–constantan, 0.0762 mm diameter wire) which was calibrated with a mercury thermometer was placed at the geometrical center of a spheroid or a fixed location (Fig. 3) in a mushroom-shaped sample.

For the freezing experiment, the whole wind tunnel unit was placed in a $-20.0 \pm 1.0°C$ walk in freezer available in the Food Science Department, Rutgers University. Temperature data were recorded in 1 or 2 min intervals by an Esterline Angus model PD-2064 digital recorder with 0.1°C resolution. Each freezing experiment was terminated when the sample temperature reached $-15°C$. The averaged superficial air velocity was measured by a KURZ portable Air Velocity Meter 440 Series at the outlet of the wind tunnel column at five specific locations (one at the center and four at the mid-point between the center and tunnel wall separated by 90°). The velocity was 5.0 m s^{-1}. For the thawing experiment, similar procedures were applied. However, the samples were kept in a $-15°C$ freezing chamber to obtain uniform initial temperature. Then, the wind tunnel was placed at a constant temperature environment ($25.0 \pm 1.0°C$). The experiments were terminated when the sample temperature reached 10°C. An average air velocity of 3.7 m s^{-1} was used in the thawing of spheroids. The value of h, convective surface heat transfer coefficient, is dependent on the environmental conditions (air flow pattern and surface characteristics) and is difficult to measure accurately, therefore it was determined by a 'curve fitting' method. However, in the radiative heat transfer, the view factor (F) was set to 1.0 because of a small object in a large enclosure [27]. Furthermore, the emissivity of Tylose gel was assumed to be 0.95 which is the emissivity of water at 0°C. An objective function used for the optimization or curve fitting was the sum of square differences (SS) between the experimental and simulation sample temperatures collected at 1 min intervals. An optimal h value was obtained by finding one specific h corresponding to the minimal SS value. This optimal h value was used to estimate the temperature history curve of another sample undergoing another similar freezing or thawing experiment. Three experiments were formed for each sample and data were reproduced well.

RESULTS AND DISCUSSIONS

Although the value of h used in the numerical simulation was not directly measured, it is possible to justify

h values used for spheroids by comparing the calculated h through using the empirical equations proposed by Smith *et al.* [28] with the present ones. It is interesting to find that h values obtained from Smith *et al.*'s formulae (convective film coefficients for acrylic plastic spheroids) with air velocities of 5.0 and 3.7 m s^{-1} are 32.6 and 25.5 W m^{-2} C^{-1}, respectively. The h values used in freezing and thawing simulations of spheroids were 37.3 and 27.0 W m^{-2} C^{-1} which are close to calculated values within 15 and 6%, respectively.

Figure 5 shows very good agreement between experimental and theoretical process temperature history curves for the freezing of a mushroom-shaped sample. The errors in the precooling peroid could be caused by the PE film which did not perfectly contact with the sample surface because of the complicated boundary. Figures 6 and 7 show the freezing and thawing results of a spheroidal sample, respectively. The temperature difference at the beginning of the tempering (freezing) period could be due to a possible error in the empirical formula for estimating the enthalpy (or apparent specific heat). The maximal temperature differences between calculated and experimental data are 2.0 and 3.2°C in the freezing of mushroom shape and spheroid, respectively. For spheroidal thawing, the maximal temperature difference is 1.0°C.

Since an analytical solution is very difficult to derive for a non-linear heat conduction equation and its corresponding initial and boundary conditions, a numerical method was considered. Unfortunately, there is no reasonable solution when the finite difference method was applied no matter how small a time increment was used. One of the unrealistic results is the calculated boundary nodal temperature being lower than the cooling medium temperature (or higher than the heating medium temperature in the thawing simulation). This problem could be caused by an unrealistic heat balance around each surface node on a curvilinear boundary when the finite difference approximation was applied since the traditional finite

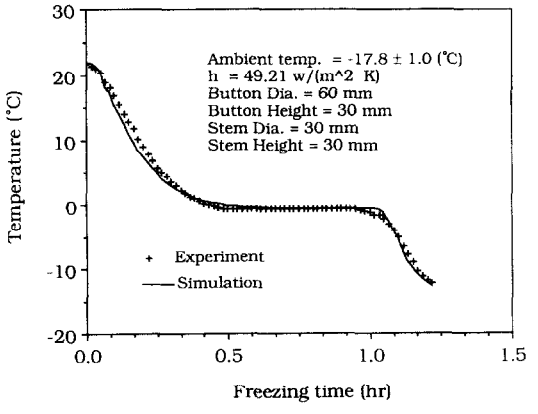

FIG. 5. Experimental vs calculated data for mushroom-shaped material (Tylose gel) during freezing process simulation.

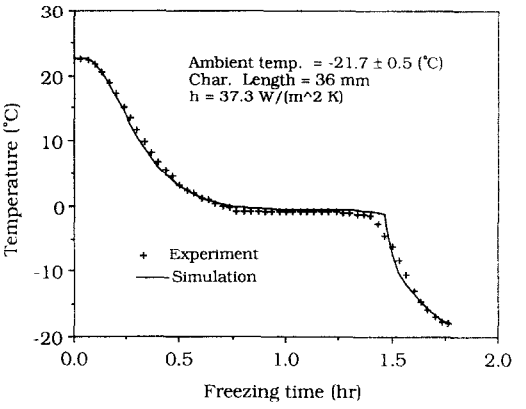

FIG. 6. Experimental vs calculated data for the freezing simulation of a spheroid at the thermal center.

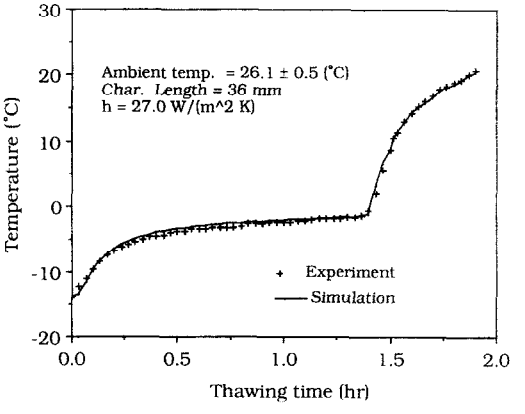

FIG. 7. Experimental vs calculated thermal center temperature history curves for the thawing of a spheroid.

difference uses a rectangular approximation. The other problem is the temperature oscillation at the boundary nodes.

However, good results were obtained after combining it with the heat balance method as described above. As for the grid nodal point designs for mushroom-shaped and spheroidal domains, it is important to make an arrangement that the nodal point spacings around the boundary should be small but large enough to save computer cost. Usually, 5% of the rotation axis length is adequate for obtaining a good solution. Moreover, the internal nodal point distance is not necessarily equal as shown, this kind of design will save computer CPU and give the flexibility of nodal point arrangement.

Iterative computations were required at each time increment as stated before. A convergence criterion used for this iterative calculation was a relative difference of two successive iterations. Temperatures estimated with convergence criteria of 1.0 and 0.1% were almost identical to each other (the nodal temperature difference is less than 0.1%). Therefore, a 1.0% relative difference was used for all the simulations. The

number of nodal points is another important factor which will affect the CPU requirement. An optimal number of nodal points for either mushroom shape or spheroid was found to be between 150 and 200 to discretize the sample domain. There was virtually no difference in estimated nodal temperature when a larger number of nodes was used. The time step for these simulations can be as large as 5 s at the initial step (can be increased by 4 times gradually as the process proceeds) and the CPU required is about 600–1000 s for one simulation using a VAX 8650.

The freezing times of a mushroom-shaped sample were estimated with assumed volumetric and no volumetric expansions (no density change). A percent difference was calculated from the simulation results (the freezing time with volumetric change less the one without volumetric change divided by the former). Figure 8 shows that the volumetric effect is about 1.1% at low Biot number (0.1) and smoothly increases to about 2.2% as Biot number increases to 40.0 (the freezing time with the expansion is longer than that without the expansion). A possible reason for this phenomenon is as follows.

With a large Biot number, a local volumetric change due to freezing proceeded faster from the surface inward as compared to a freezing process with a low Biot number. Therefore, the influence of volumetric change on freezing time is more significant for a high freezing rate although the influence is negligibly small for the practical purpose.

An expansion factor in the axis of the spheroid was found to be about 2% when the geometric center reached −20°C based on the freezing simulation which resulted in a 6.12% volumetric expansion. Since the freezing volumetric expansion of pure water is about 9%, the 6.12% calculated result for a 77% moisture content material is reasonable.

CONCLUSION

A mathematical model with volumetric changes during a phase change (freezing/thawing) process was formulated by modifying the heat conduction partial differential equation. To solve this model numerically, a new numerical scheme for an irregular domain was developed by applying the finite difference and finite volume heat balance methods. The simulation results for the freezing of mushroom-type and freezing/thawing of spheroid samples show very good agreement with the experimental data. The influence of the volumetric expansion effect on freezing time estimation of high moisture content food materials was about 2% which is not significant for the practical purpose.

The developed computer package can be applied to general heat conduction processes with phase change (solidification and melting) and applied to materials of high moisture content thermal processes.

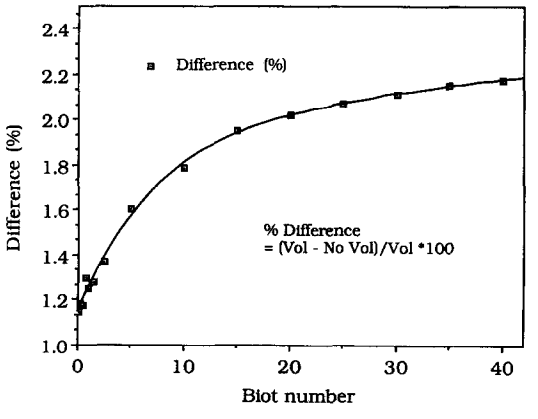

FIG. 8. The volumetric effect on freezing time calculation (Tylose gel, mushroom shape, 77% moisture, for temperature down to −10.0°C).

Acknowledgements—New Jersey Agricultural Experiment Station, Publication No. D10103-2-91, supported in part by U.S. Hatch Act Fund. Mainframe computer time fund was provided by Rutgers University Center for Computer and Information Services and Supercomputer time fund was provided by the John Van Neumann National Supercomputer Center, Princeton, NJ 08543, U.S.A.

REFERENCES

1. L. N. Tao, The heat conduction problem with temperature-dependent material properties, *Int. J. Heat Mass Transfer* **32,** 487–491 (1989).
2. M. N. Ozisik, *Heat Conduction*, pp. 397–438. Wiley, New York (1980).
3. H. S. Carslaw and J. C. Jaeger, *Conduction of Heat in Solids*, 2nd Edn. Oxford University Press, London (1959).
4. D. R. Lynch and K. O'Neil, Continuously deforming finite elements for the solution of parabolic problems, with and without phase change, *Int. J. Numer. Meth. Engng* **17,** 81–96 (1981).
5. J. Yoo and B. Rubinsky, Numerical computation using finite elements for the moving interface in heat transfer problems with phase transformation, *Numer. Heat Transfer* **6,** 209–222 (1983).
6. Q. T. Pham, A fast, unconditionally stable finite difference scheme for heat conduction with phase change, *Int. J. Heat Mass Transfer* **28,** 2079–2084 (1985).
7. N. Shamsundar and E. Rooz, Numerical methods for moving boundary problems. In *Handbook of Numerical Heat Transfer* (Edited by W. J. Minkowycz, E. M. Sparrow, G. E. Schneider and R. H. Pletcher), pp. 747–768. Wiley, New York (1988).
8. T. Saitoh and H. Kato, A probabilistic numerical method for heat transfer problem—application to phase change problem. In *Transport Phenomena in Thermal Control* (Edited by G.-J. Hwang), pp. 665–676. Hemisphere, New York (1989).
9. A. K. Fleming, The numerical calculation of freezing processes. In *Progress in Refrigeration Science and Technology* (Edited by XIII Int. Congress of Refrigeration), Vol. 2, pp. 303–311. AVI, Connecticut (1973).
10. H. K. Purwadaria and D. R. Heldman, A finite element model for prediction of freezing rates in food products with anomalous shapes, *Trans. ASAE* **25,** 827–832 (1982).
11. K. Hayakawa, C. Nonino, J. Succar, G. Comini and S. D. Giudice, Two dimensional heat conduction in food undergoing freezing: development of computerized model, *J. Fd Sci.* **48,** 1849–1853 (1983).
12. J. Succar and K. Hayakawa, Parametric analysis for

predicting freezing time of infinitely slab-shaped food, *J. Fd Sci.* **49,** 468–477 (1984).
13. C. Bonacina and G. Comini, On the solution of the non-linear heat conductions by numerical methods, *Int. J. Heat Mass Transfer* **16,** 581–589 (1973).
14. J. D. Mannapperuma and R. P. Singh, Prediction of freezing and thawing times of foods using a numerical method based on enthalpy formulation, *J. Fd Sci.* **53,** 626–630 (1988).
15. Q. T. Pham, A converging-front model for the asymmetric freezing of slab-shaped food, *J. Fd Sci.* **52,** 795–800 (1987).
16. A. C. Cleland and R. L. Earl, Prediction of freezing times for foods in rectangular packaging, *J. Fd Sci.* **44,** 964–970 (1979).
17. D. J. Cleland, A. C. Cleland, R. L. Earl and S. J. Byrne, Prediction of freezing and thawing times for multi-dimensional shapes by numerical methods, *Int. J. Refrig.* **10,** 32–39 (1987).
18. J. R. Welty, *Engineering Heat Transfer*, pp. 45–48. Wiley, New York (1974).
19. J. R. Rosenau, Analysis of freezing and thawing using techniques for solving stiff systems of differential equations, Internal Report, Food Engng Dept., University of Massachusetts, Amherst (1977).
20. G. Comini and S. Del Giudice, Thermal aspects of cryosurgery, *J. Heat Transfer* **98,** 543–549 (1976).
21. Anonymous, Cooling and freezing times of food. In *ASHRAE Fundamentals Handbook*, Chap. 30:30.1. ASHRAE, Atlanta, Georgia (1981).
22. D. W. Peaceman and H. H. Rachford, Jr., The numerical solution of parabolic and elliptic differential equations, *J. Soc. Ind. Appl. Math.* **3,** 28–41 (1955).
23. G. D. Smith, *Numerical Solution of Partial Differential Equations, Finite Difference Methods*, 2nd Edn, pp. 11–41. Clarendon Press, Oxford (1978).
24. S. Sheen, Parametric analysis of non-linear, two dimensional, transit state heat conduction in food undergoing freezing and thawing with volumetric changes, Ph.D. Thesis, Rutgers University, New Jersey (1990).
25. R. M. Furzeland, A comparative study of numerical methods for moving boundary problems, *J. Inst. Math. Appl.* **26,** 411–429 (1980).
26. L. A. Riedel, Eine prufsubstanz fur gefrierversuche, *Kaltetechnik* **12,** 222–225 (1960).
27. C. J. Geankoplis, *Transport Process and Unit Operations*, 2nd Edn, pp. 258–262. Allyn & Bacon, Boston (1983).
28. R. E. Smith, A. H. Bennett and A. A. Vacinek, Convection film coefficients related to geometry for anomalous shapes, *Trans. ASAE* **14,** 44–47 (1971).

SIMULATION PAR DIFFERENCES FINIES DE LA CONDUCTION THERMIQUE AVEC CHANGEMENT DE PHASE DANS UN DOMAINE IRREGULIER ET AVEC CHANGEMENT DE VOLUME

Résumé—Un modèle mathématique incluant les changements de volume pour la congélation d'aliment est obtenu en modifiant l'équation générale de la conduction thermique, parabolique aux dérivées partielles. La forme de l'aliment est supposée être axiale avec un contour irrégulier en section droite. Les coordonnées sont fixées au volume initial par une transformation de coordonnées appropriée. A cause de la forte variation des propriétés avec la température pendant le changement de phase, les températures nodales sont résolues numériquement par une méthode générale implicite aux différences finies, tandis qu'une méthode de bilan thermique est appliquée aux frontières des noeuds avec des conditions aux limites d'espèce quelconque. Une méthode de calcul numérique est développée et elle est vérifiée expérimentalement par un problème général de changement de phase (solidification/fusion).

SIMULATION DER WÄRMELEITUNG MIT PHASENWECHSEL IN EINEM UNREGELMÄSSIG GEFORMTEN LEBENSMITTEL MIT VOLUMENÄNDERUNG

Zusammenfassung—Ein mathematisches Modell, das die Volumenänderung während des Gefrierens und des Auftauens von Lebensmitteln berücksichtigt, wird durch Modifizieren der allgemeinen partiellen parabolischen Differentialgleichung der Wärmeleitung erhalten. Die Gestalt des Lebensmittels wird als Rotationskörper mit unregelmäßiger Kontur angenommen. Die Koordinaten sind mit dem ursprünglichen Lebensmittelvolumen über eine geeignete Koordinatentransformation verknüpft. Aufgrund der starken Temperaturabhängigkeit der Lebensmitteleigenschaften während des Phasenwechsels werden die Temperaturen der Knotenpunkte numerisch mit einem allgemeinen impliziten Differenzenverfahren berechnet. An den Randknotenpunkten wird hingegen eine Wärmebilanzmethode mit beliebiger Art von Randbedingungen angewandt. Es wird eine rechnerunterstützte numerische Simulation entwickelt und experimentell für ein allgemeines Wärmeleitungsproblem mit Phasenwechsel (Erstarren/Schmelzen) verifiziert.

ИСПОЛЬЗОВАНИЕ МЕТОДА КОНЕЧНЫХ РАЗНОСТЕЙ ДЛЯ МОДЕЛИРОВАНИЯ ТЕПЛОПРОВОДНОСТИ ПРИ НАЛИЧИИ ФАЗОВОГО ПРЕВРАЩЕНИЯ В ЧАСТИЦАХ

Аннотация—В результате модификации общего параболического уравнения теплопроводности получена математическая модель, учитывающая объемные изменения при замораживании или оттаивании пищевых продуктов. Частица пищевых продуктов рассматривается как тело вращения с поперечным сечением неправильной формы. С помощью проведения соответствующего преобразования вводятся координаты, связанные с начальным объемом. Поскольку свойства частиц в процессе фазового превращения в значительной степени зависят от температуры, уравнения решаются численно конечно-разностным методом с неявной схемой, в то время как метод теплового баланса используется в граничных узлах сетки при любых граничных условиях. Разработан и экспериментально подтвержден метод численного моделирования общей задачи теплопроводности при фазовом превращении (затвердевание/таяние).